Substrate Binding and Reduction of Benzoyl-CoA Reductase: Evidence for Nucleotide-Dependent Conformational Changes†

Henrik Möbitz,‡,§ Thorsten Friedrich,|| and Matthias Boll*,‡

Institut für Biologie II, Mikrobiologie, Universität Freiburg, Schänzlestrasse 1, and Institut für Organische Chemie und Biochemie, Universität Freiburg, Albertstrasse 21, D-79104 Freiburg, Germany

Received October 21, 2003; Revised Manuscript Received November 25, 2003

ABSTRACT: Benzoyl-CoA reductase (BCR) from the denitrifying bacterium *Thauera aromatica* catalyzes the ATP driven two-electron reduction of the aromatic moiety of benzoyl-CoA (BCoA) to a nonaromatic cyclic diene (2 ATP/2 e^-). The enzyme contains two similar but nonidentical ATP-binding sites of the acetate kinase/sugar kinase/Hsp70/actin family. To obtain further insights into the overall catalytic cycle of BCR, the binding affinities and stoichiometries of all substrates as well as their effects on reduction kinetics were studied by stopped-flow UV/vis spectroscopy, freeze−quench EPR spectroscopy, and equilibrium dialysis. BCR bound maximally two nucleotides and a single BCoA. The binding of a single nucleotide induced a molecular switch (BCR → BCR*) as evidenced as follows: (i) the reduction rate of BCR by sulfoxide radical anion was significantly decreased in the nucleotide-bound state, (ii) the binding of BCoA to the reduced enzyme strictly depended on bound nucleotides, and (iii) the nucleotide binding affinities increased up to 60-fold compared to the steady-state values. The "ATP-binding switch" is distinguished from the previously described "low-spin/high-spin switch" of a [4Fe-4S] cluster which strictly depends on ATP hydrolysis. The two nucleotide binding sites were occupied sequentially; binding constants of the two sites differed by a factor of 10−40. The kinetic data obtained suggest that the ATP-binding switch is a rather fast process (>100 s^{-1}) with a switch equilibrium constant of 54 ± 10. In contrast, the reverse switch back of the MgADP-bound enzyme (BCR* → BCR) is considered rate-limiting in the overall catalytic cycle of BCR (4 ± 1 s^{-1}). The binding of nucleotides did not affect the redox potential of the [4Fe-4S]$^{+1/+2}$ clusters; the switch is rather considered to alter the kinetics of internal electron transfer. Implications for the overall catalytic cycle of benzoyl-CoA reductase are discussed and compared with other ATP-hydrolyzing enzymes.

Benzoyl-CoA reductase (BCR)[1] catalyzes a central step in the anoxic metabolism of aromatic compounds in bacteria: the reductive dearomatization of benzoyl-CoA (BCoA) to cyclohexa-1,5-diene-1-carbonyl-CoA (ChdCoA; *1*, *2*). The transfer of two electrons from ferredoxin to the substrate is coupled to the hydrolysis of two ATP to ADP (*3*−*5*; Figure 1). Substrate reduction is proposed to proceed in a Birch-like mechanism, in which the proton-assisted transfer of the first electron yielding a cyclohexadienyl radical represents a rate-governing step (*6*). The reaction catalyzed by BCR shares similarities with that of nitrogenase. Both enzymes use the hydrolysis of ATP to overcome the substantial kinetic and thermodynamic barriers posed by the reduction of very stable molecules. Despite these analogies, BCR and nitrogenase have no amino acid sequence homology.

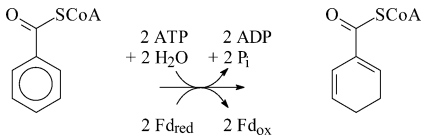

FIGURE 1: Reaction catalyzed by benzoyl-CoA reductase from *T. aromatica*. BCoA is reduced by two electrons which are supplied by ferredoxin; 2 ATP per 2 e^- transferred are hydrolyzed.

So far, the biochemistry of BCR has exclusively been studied in the denitrifying bacterium *Thauera aromatica*. The heterotetrameric (ABCD composition) 170 kDa protein contains three [4Fe-4S] clusters (*5*; Figure 2). The B- and C-subunits of BCR have amino acid sequence similarities to two subunits of 2-hydroxyglutaryl-CoA dehydratase; the A- and D-subunits, to its homodimeric electron activating enzyme, termed activase in the following (*7*). The latter enzyme catalyzes an ATP-dependent activation of electrons, which are required for the difficult water elimination from 2-hydroxyacyl-CoA thiol esters (*8*). Buckel and Keese (*9*) proposed that BCR and 2-hydroxyglutaryl-CoA dehydratase catalyze similar reactions by means of ketyl radical intermediates. The crystal structure of activase revealed a

† This work was supported by grants from the Deutsche Forschungsgemeinschaft (BO 1565, 3-2).

* Corresponding author. Tel: 49 7612032685. Fax: 49 7612032626. E-mail: boll@uni-freiburg.de.

‡ Institut für Biologie II, Mikrobiologie, Universität Freiburg.

§ Present address: Department for Chemistry and Biochemistry, University of California, Santa Barbara, Santa Barbara, CA 93106.

|| Institut für Organische Chemie und Biochemie, Universität Freiburg.

[1] Abbreviations: BCoA, benzoyl-CoA; BCR, benzoyl-CoA reductase; BCR_{ox}, thionine-oxidized benzoyl-CoA reductase; BCR_{red}, dithionite-reduced benzoyl-CoA reductase; Fd, ferredoxin; SFS, stopped-flow UV/vis spectroscopy; ChdCoA, cyclohexa-1,5-diene-1-carbonyl-CoA; Mops, 3-(*N*-morpholino)propanesulfonic acid.

10.1021/bi0358871 CCC: $27.50
Published on Web 01/16/2004

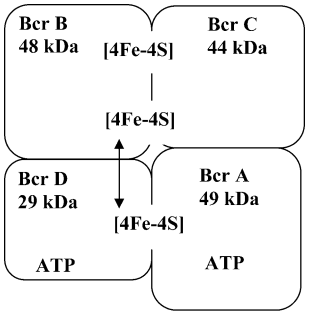

FIGURE 2: Proposed molecular architecture of benzoyl-CoA reductase. The model is based on spectroscopic studies and on amino acid sequence similarity with the two-component system 2-hydroxyglutaryl-CoA dehydratase/activase of *A. fermentans* (*7*, *10*). The arrow indicates a magnetic interaction between clusters I and II.

molecular architecture analogous to the Fe protein of nitrogenase (*10*). In analogy, we distinguish between a substrate reduction module and an electron activating module. The latter is formed by the A- and D-subunits, containing one ATP-binding site each and an interfacially coordinated [4Fe-4S] cluster (Figure 2). The ATP-binding sites of BCR belong to the ASKHA family (acetate and sugar kinase/heat shock protein 70/actin), comprising enzymes that catalyze ATP hydrolysis or phosphoryl transfer coupled to large conformational changes (*11*). Amino acid sequence analysis revealed that the ATP-binding sites of BCR are similar to each other though not identical (*7*, *12*). The asymmetric architecture of the electron activating module is also reflected in the largely differing masses of the A- and D-subunits (Figure 2). The substrate reduction module is formed by the remaining subunits of BCR (B and C), which carry two further [4Fe-4S] clusters; this module is supposed to bind BCoA.

The three [4Fe-4S] clusters of BCR were characterized by EPR and Mössbauer spectroscopy (*4*, *5*). In the dithionite-reduced state a major broad EPR signal is observed at temperatures below 10 K, which is assigned to two magnetically interacting $[4Fe\text{-}4S]^{+}$ clusters. Nucleotide binding was shown to decrease this interaction, indicating a conformational change (*5*). In addition, dithionite-reduced BCR displays minor EPR signals (total spin ~0.2 spin/enzyme), which derive from noninteracting $[4Fe\text{-}4S]^{+}$ clusters, termed I and II with $E'^{\circ} < -500$ mV. A complex third EPR signal III was putatively assigned to a third cluster interacting with an unknown paramagnet; its nature is still at issue.

Recently, insights into the ATP-hydrolysis-dependent events in the catalytic cycle of BCR have been obtained. The following steps can be distinguished: (i) formation of an energy-rich enzyme−phosphate from ATP, (ii) a redox-dependent autodephosphorylation (*13*), and (iii) the switch of one $[4Fe\text{-}4S]^{+1}$ cluster from the $S = {}^{1}/_{2}$ low-spin state into an unusual $S = {}^{7}/_{2}$ high-spin state (*4*, *5*). The order of the last two events remains to be established. In single-turnover EPR experiments, the low-spin/high-spin switch occurred reversibly in the catalytic cycle of BCR, supporting its catalytic relevance (*14*). The formation of the high-spin state can be explained by a displacement of one Fe atom into the $[4Fe\text{-}4S]^{+}$ cluster driven by a conformational change; calculations revealed that such a switch could lower the redox potential of a $[4Fe\text{-}4S]^{+1}$ cluster by up to −500 mV (*15*).

The present work addresses the unknown binding affinities/stoichiometries of the individual substrates and substrate binding induced conformational changes in BCR. The results obtained from stopped-flow UV/vis spectroscopy (SFS), freeze−quench EPR spectroscopy, and equilibrium dialysis studies indicate that nucleotide-dependent conformational changes govern the catalytic cycle of BCR.

EXPERIMENTAL PROCEDURES

Materials. [*ring*-^{14}C]Benzoic acid was purchased from American Radiolabeled Chemicals Inc.; [8-^{14}C]adenosine 5′-diphosphate and [8-^{14}C]adenosine 5′-triphosphate were obtained from Hartmann Analytic GmbH, Germany. The specific activities were 4760 MBq/mmol (BCoA), 2016 MBq/mmol (ADP), and 2090 MBq/mmol (ATP).

Growth of Bacterial Cells. T. aromatica (DSM 6984) was grown anoxically at 28 °C in a mineral salt medium. 4-Hydroxybenzoate and nitrate in a ratio of 1:3.5 served as sole sources of energy and cell carbon. Continuous feeding of the substrates, cell harvesting, storage, and preparation of cell extracts were carried out as described previously (*16*).

Protein Purification and Sample Preparation. Purification of BCR from *T. aromatica* (wet cell mass 200 g) was performed under strictly anaerobic conditions in a glovebox under a N_2/H_2 atmosphere (95:5 v/v) at 6−10 °C as described earlier (*3*). The enzyme used throughout this study was more than 90% pure. Enzyme activity was routinely determined in the previously described spectrophotometric assay following the substrate- and enzyme-dependent oxidation of reduced methyl viologen (*3*). Protein aliquots (in 20 mM triethanolamine, pH 7.3, 4 mM $MgCl_2$, 180 mM KCl, 10% glycerol, and 0.5 mM dithionite) were stored in liquid nitrogen without loss of activity over several months.

"Oxidized enzyme" (BCR_{ox}) was freshly prepared in the anaerobic glovebox by titration with an anaerobically prepared stock solution of a saturated thionine solution (approximately 10 mM) in 150 mM Mops/KOH and 10 mM $MgCl_2$, pH 7.3, referred to as reaction buffer. Oxidant and salt were quantitatively removed by passing the enzyme over a Sephadex G-25 column (~5 mL bed volume, 1 cm diameter; Amersham Pharmacia), which had been equilibrated with reaction buffer. Completeness of enzyme oxidation was shown by the inability of the BCR solution to reduce oxidized methyl viologen. Under the conditions described above, the reduction properties of BCR were fully maintained for at least 24 h at 20 °C.

"Reduced enzyme" (BCR_{red}) refers to BCR_{ox} which was reduced with fresh dithionite (typically 100 μM in reaction buffer).

Synthesis and Purification of BCoA. BCoA was synthesized from CoA and benzoic acid anhydride (*17*). Purification and purity control were by HPLC as described earlier (*6*). [*ring*-^{14}C]-BCoA was prepared enzymatically using partially purified benzoyl-CoA synthetase from *T. aromatica*; purification of the thiol ester was by reversed-phase C_{18} extraction as described earlier (*18*).

Equilibrium Dialysis. All equilibrium dialysis experiments were performed in a glovebox under strictly anaerobic conditions (N_2/H_2 atmosphere, 95:5 v/v). The custom-built acrylic equilibrium dialysis glass cell had two compartments of 180 μL each, separated by a 10 kDa cutoff standard

dialysis membrane. Using a Hamilton syringe, the individual compartments were filled with 180 μL of BCR and 180 μL of ^{14}C-labeled ligand (~5 MBq), respectively. Both the enzyme and the ligand were in reaction buffer (dithionite and DTE were added as stated below). The cell was sealed with tape and rotated at 4 °C. Dialysis equilibrium was reached after ~21 h. After 24 h, two 50 μL aliquots were removed from each compartment, and the concentrations of bound ^{14}C-labeled ligand were determined by liquid scintillation counting. For the determination of the high ($K_{d,1}$) and low affinity ($K_{d,2}$) of the nucleotide binding sites, two different enzyme concentrations were used (typically 30 and 100 μM).

Due to the sensitivity of BCR to oxygen damage and the sensitivity of BCoA to hydrolysis, the dialysis time in experiments involving BCoA and/or oxidized enzyme was reduced to 12 h in order to minimize exposure. To ensure that equilibrium was reached within this period, equal amounts of the radioactively labeled ligand were added to both compartments at the beginning of the experiment; controls verified that under these conditions dialysis equilibrium was reached after 10 h. When oxidized enzyme was studied, the addition of 2 mM DTE had a protective effect on the enzyme. Under these conditions, 85% of the initial reductase activity were retained after the experiment. Note that the midpoint potential of DTE is too high to transfer electrons to BCR (*5*). When [*ring*-^{14}C]-BCoA was tested as a ligand, the experiments were performed at pH 7.0 in reaction buffer in order to minimize hydrolysis. According to analytical HPLC, 10% of the initially added BCoA was hydrolyzed under these conditions. Concentrations were corrected for substrate hydrolysis.

Stopped-Flow Instrumentation and Measurement. Stopped-flow UV/vis experiments were carried out in a custom-built stopped-flow apparatus, installed in a glovebox under a strictly anaerobic N_2/H_2 (95:5 v/v) atmosphere. All samples were prepared and handled inside the glovebox. The apparatus was equipped with two syringes that were driven by pressurized gas (N_2/H_2, 95:5 v/v). The optical cell (30 μL volume, 10 mm path length) was connected to two light carriers, one leading to the deuterium/halogen lamp and the other to a TIDAS I diode array spectrophotometer (J&M, Aalen, Germany). Single UV/vis absorption spectra were recorded on the same system by connecting the light carriers to a cuvette holder (J&M). Injection and mixing of the samples (less than 10 ms dead time) triggered the recording of stopped-flow data sets. In a typical experiment, the integration time was 10 ms, and approximately 100 spectra were taken between 0 and 6000 ms. Data storage and handling were carried out on a personal computer with the Spectralys 1.81 software package (J&M). One set of injections (2 mL sample) yielded at least six similar data sets that were averaged for further analysis. The concentration of BCR was usually in the range of 20 μM. ATP, ADP, BCoA, and sodium dithionite concentrations were varied as indicated. Concentrations of BCR, nucleotides, and dithionite were determined photometrically as described below. In all experiments enzyme and ligand were in the reaction buffer. The temperature of the syringes and the optical cell was kept constant at 20 ± 1 °C by a circulating water bath.

Analysis of Kinetic Data. Rate constants were obtained by fitting the recorded data to exponential functions using least-squares minimization and global fitting (VEEspec6 software program by Dr. Friedel Drepper, University of Freiburg). The rates thus obtained were plotted and fitted to the corresponding equations with the PRISM software package (GraphPad Software, Inc.). Kinetic simulations were performed with the sysrk software (Dr. Friedel Drepper, University of Freiburg) by changing the rate to be determined so as to fit the $k_{obs,fast}$ of the fast phase of dithionite reduction. Differential equations were programmed according to the reaction scheme in Figure 7. In these simulations, sulfoxide reduction was treated as a pseudo-first-order reaction using the k_{obs} obtained for free and nucleotide-bound enzyme, k_3' and k_4'(see Results for definition). The preceding dissociation of dithionite to the sulfoxide radical could be neglected; inspection of the dissociation rate of dithionite (1.7 s^{-1}; *25*) and the second-order reduction rate determined for BCR_{ox} (see below) shows that it is not rate-limiting even at equimolar ratios of BCR_{ox} and dithionite.

Analysis of Equilibrium Dialysis Binding Data. The data were fitted directly to three equations using the PRISM software package (GraphPad Software, Inc.) in order to test different binding models. Manual global analysis was performed to maximize the fit (judged by r^2). The following equations were used for binding to two identical sites (eq 1), binding to two sites with differing affinities (eq 2), and sequential binding to two sites with differing affinities (eq 3), where [X] is the concentration of free nucleotide and r is the fraction of the enzyme with bound nucleotide.

$$r = n_1[X]/([X] + K_d) \quad (1)$$

$$r = n_1[X]/([X] + K_{d,1}) + n_2[X]/([X] + K_{d,2}) \quad (2)$$

$$r = n_1[X]/([X] + K_{d,1}) + n_2([X]/([X] + K_{d,1}))([X]/([X] + K_{d,2})) \quad (3)$$

Equation 3 corresponds to the reaction scheme shown in Figure 7.

Freeze−Quench X-Band EPR Spectroscopy. For freeze−quench experiments, conditions were chosen in order to reproduce the kinetics of the SFS-monitored dithionite reduction of BCR. Two gastight syringes were filled with 260 μM oxidized BCR (prepared as described above; 30 min incubation with excess thionine) and with a freshly prepared 2.6 mM sodium dithionite solution, respectively. Mixing was carried out with a manual device with a mixing temperature of 20 °C; rapid freezing was accomplished by placing an EPR tube into isopentane cooled by liquid nitrogen to ~135 K. The minimal time between mixing and freezing was estimated to be approximately 0.5 s. EPR measurements were conducted with a Bruker EMX 1/6 spectrometer operating at X-band (9.2 GHz). The sample temperature was controlled with an Oxford Instrument ESR-9 helium-flow cryostat. The magnetic field was calibrated using a strong or a weak pitch standard. EPR conditions are described in the legends to the individual figures.

Further Determinations. Substrate and protein concentrations were determined spectrophotometrically (at least triple determination) using the following absorption coefficients: ϵ_{314nm} = 8 mM^{-1} cm^{-1} for dithionite (*20*), ϵ_{260nm} = 15.4 mM^{-1} cm^{-1} for ATP and ADP (*20*), ϵ_{260nm} = 21.6 mM^{-1} cm^{-1} for BCoA (*21*), and ϵ_{280nm} = 165 mM^{-1} cm^{-1} for BCR

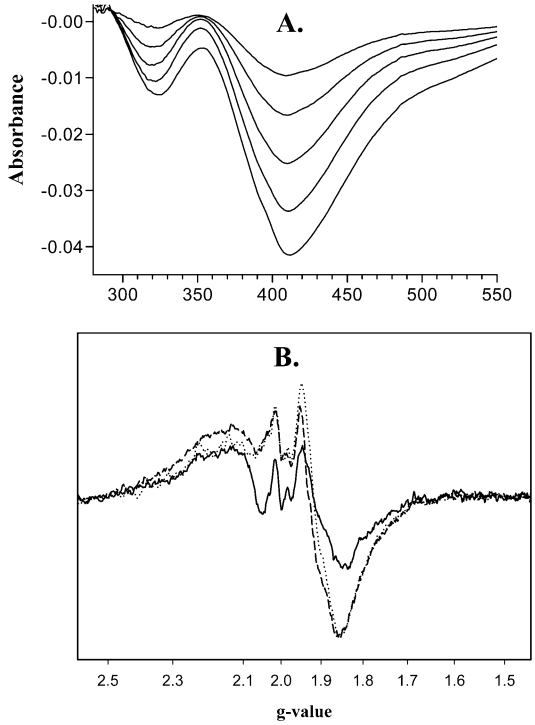

FIGURE 3: Stopped-flow UV/vis spectroscopy and freeze−quench EPR spectroscopy of dithionite reduction of thionine-oxidized BCR. (A) UV/vis difference spectra taken at 60, 120, 260, 1000, and 6000 ms (from top to bottom) after the mixing of BCR_{ox} (29 μM) and dithionite (256 μM). The proportion of the dithionite spectrum has been subtracted. (B) EPR spectra of thionine-oxidized BCR (130 μM) reduced by dithionite (1.3 mM). Spectra were recorded after mixing of equal volumes of enzyme and dithionite for 0.5 s (solid line), 5 s (dotted line), and 60 s (dashed line). For preparation of samples, see Experimental Procedures. EPR parameters: microwave frequency, 9459 MHz; microwave power, 20 mW; modulation amplitude, 1.2 mT; temperature, 5 K.

(this work). Protein concentration was also determined according to Bradford, using BSA as the standard (*22*). Purity control of BCR was by SDS gel electrophoresis (*23*); protein concentrations were corrected for the purity of the enzyme.

RESULTS

Reduction Kinetics of Oxidized Benzoyl-CoA Reductase in the Absence of Substrates. The reduction kinetics of thionine-oxidized BCR by the artificial electron donor dithionite was investigated by quantitative stopped-flow UV/vis spectroscopy and qualitative freeze−quench EPR spectroscopy. The kinetic data obtained should reveal MgATP-, MgADP-, and BCoA-induced conformational changes affecting the extent and/or rate of BCR reduction.

The reduction of BCR was monitored by stopped-flow UV/vis spectroscopy by following the time-dependent decrease in absorption at 410 nm that is due to bleaching of [4Fe-4S] clusters (for absorption spectra of BCR, see ref *3*). Difference spectra at various time points obtained after the subtraction of the dithionite spectrum are shown in Figure 3A. The difference spectrum had two maxima at 410 and 323 nm; the difference absorbance coefficients were calculated as $\Delta\epsilon_{410nm} = 7.4\ mM^{-1}\ cm^{-1}$ and $\Delta\epsilon_{324nm} = 2.7\ mM^{-1}\ cm^{-1}$. Both the shape of the spectrum and the ratio of the two maxima were characteristic for two interacting [4Fe-4S] clusters as observed in ferredoxins or NADH:ubiquinone

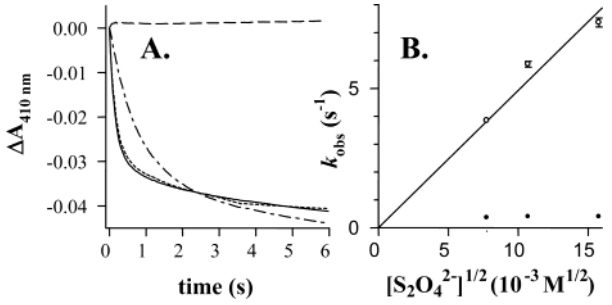

FIGURE 4: Kinetics of BCR_{ox} reduction by dithionite as determined by stopped-flow UV/vis spectroscopy. (A) Stopped-flow UV/vis spectroscopy reaction trace at 415 nm showing the bleaching of the BCR_{ox} spectra by dithionite reduction in Figure 3A. The reaction trace of BCR_{ox} reduction (29 μM) by dithionite (256 μM) is in the absence of a substrate (—). Reaction mixtures additionally contained 200 μM BCoA (- - -) or 250 μM ATP (— · —); BCR_{red} (in the presence of 128 μM dithionite) was mixed with 500 μM ADP/128 μM dithionite (— —). (B) Concentration dependence of the two phases of dithionite reduction of BCR_{ox} (9.9 μM final concentration). The k_{obs} are plotted against the square root of dithionite concentration. The fast phase (○) gives a linear relation through the origin ($r^2 = 0.98$); the slow phase (●) shows no significant dependence on the dithionite concentration.

oxidoreductase (*24*). In the course of the reaction, the enzyme could be reduced by 0.4−0.5 electron.

The reduction of BCR by dithionite was also followed by manual freeze−quench EPR spectroscopy. For this purpose BCR was rapidly mixed with dithionite and frozen at approximately 0.5, 5, and 60 s. Figure 3B shows the broad EPR spectra of two interacting [4Fe-4S] clusters recorded at 5 K as described earlier (*4*, *5*). From 0.5 to 5 s the overall signal intensity increased by a factor of 2.6 as estimated from the increase of the maximal amplitude of the signal. However, it did not increase further between the 5 and 60 s incubation with dithionite, indicating that reduction was completed after 5 s of the reaction. This time course is in qualitative agreement with the corresponding SFS experiment (see Figure 4A). Note that the determination of the absolute spin concentration is not feasible due to the broad EPR signals. The spectra of noninteracting clusters recorded at 25 K showed a similar relative increase but at a much lower extent (<0.1 spin/enzyme; not shown). In addition, signals assigned to signal III (<0.1 spin/enzyme) were observed (*5*), which did not change significantly in the time course of the reaction (not shown). The results obtained from EPR spectroscopy indicate that the bleaching of the UV/vis spectrum upon dithionite reduction is mainly due to the reduction of the magnetically interacting [4Fe-4S] cluster. This suggestion is conclusive with the characteristic difference UV/vis spectra of interacting $[4Fe\text{-}4S]^+$ clusters (Figure 3A). Note that the E'° of the noninteracting [4Fe-4S] clusters is below −500 mV (*5*), which thermodynamically precludes a complete reduction by dithionite ($E'^\circ = -440$ mV at pH 7.0; *25*). The replacement of dithionite by titanium(III) citrate as reductant did not affect the extent of reduction; instead, reduction kinetics determined by UV/vis spectroscopy were even slower.

The reduction kinetics of BCR by dithionite as monitored by SFS showed a biphasic slope, which could be fitted to a sum of two exponentials (Figure 4A): in a typical experiment, in which 14.6 μM BCR and 128 μM dithionite were mixed, the fast reduction phase corresponded to a pseudo

Table 1: Kinetic, Binding, and Equilibrium Constants Used in This Work[a]

constant	description	value	origin
K_1(ADP)	steady-state affinity	1100 μM	$=K_i$ (*3*)
K_1(ATP)	steady-state affinity	600 μM	$=K_m$ (*3*)
$K_{d,1}$(ADP)	pre-steady-state affinity	32 ± 3 μM	SFS
$K_{d,1}$(ATP)	pre-steady-state affinity	11 ± 2 μM	SFS
K_2(ADP)	switch equilibrium	34 ± 3	$=K_i/K_{d,1}$(SFS)
K_2(ATP)	switch equilibrium	54 ± 10	$=K_m/K_{d,1}$(SFS)
k_{+2}(ADP)	ADP binding switch forward	136 ± 46 s^{-1}	$=k_{-2}K_2$
k_{-2}(ADP)	ADP binding switch back	4 ± 1 s^{-1}	simulation
k_{+2}(ATP)	ATP binding switch forward	135 ± 54 s^{-1}	simulation
k_3	reduction of BCR_{ox}	$(2.6 \pm 0.1) \times 10^6$ M^{-1} s^{-1}	initial velocity
k_4(ADP)	reduction of BCR_{ox}*(ADP)	$(6.3 \pm 0.1) \times 10^5$ M^{-1} s^{-1}	initial velocity
k_4(ATP)	reduction of BCR_{ox}*(ATP)	$(5.3 \pm 0.1) \times 10^5$ M^{-1} s^{-1}	initial velocity
k_4(BCoA)	reduction of BCR_{ox}*(BCoA)	$(2.4 \pm 0.5) \times 10^6$ M^{-1} s^{-1}	initial velocity

[a] The constants refer to the reaction scheme in Figure 7.

first-order rate, $k_{obs,fast}$, of 6.4 ± 0.1 s^{-1} and the slow reduction phase to a $k_{obs,slow}$ of 0.39 ± 0.01 s^{-1}. To characterize these two phases, we measured the dependence of BCR reduction on the dithionite concentration. At $[S_2O_4^{2-}]$ below 300 μM, $k_{obs,fast}$ formed a linear relation with the square root of $[S_2O_4^{2-}]$ (Figure 4B); above 300 μM $S_2O_4^{2-}$, reduction rates leveled off. This result establishes that not dithionite but the sulfoxide radical anion, $SO_2^{\bullet-}$, is the reducing species, a finding that has been reported for a great number of redox proteins (*25*−*27*, *29*). In these cases, reduction is preceded by a rapid dissociation equilibrium of $S_2O_4^{2-}$ into two $SO_2^{\bullet-}$ (accordingly, $[SO_2^{\bullet-}]$ is given by the square root of $K_d[S_2O_4^{2-}]$, with $K_d = 1.4$ nM; *25*). Similar square root dependencies were found for the reduction rates of substrate-bound BCR_{ox} (data not shown).

However, due to the substoichiometric reduction, the second-order reduction rate of BCR_{ox} cannot be derived from $k_{obs,fast}$, which only reflects attainment of the redox equilibrium. Instead, reduction is described by the following redox equilibrium (for a more detailed treatment of dithionite reduction kinetics, refer to ref *25*):

$$BCR_{ox} + SO_2^{\bullet-} \rightleftharpoons BCR_{red} + SO_2 \quad (4)$$

$$-d[BCR_{ox}]/dt = k_{+3}[SO_2^{\bullet-}][BCR_{ox}] - k_{-3}[SO_2][BCR_{red}] \quad (5)$$

A summary of rate and equilibrium constants used in this paper is given in Table 1; k_{+3} is defined as the kinetic constant of BCR_{ox} reduction by the sulfoxide radical anion. To obtain k_{+3}, initial velocities have to be used, giving a $k_{+3} = (2.6 \pm 0.01) \times 10^6$ M^{-1} s^{-1} (from $\Delta A_{410nm}/\Delta t$ during the linear reaction course in the first 80 ms, using the ϵ_{410nm} calculated above). However, because of the numerical inaccuracy associated with determining initial velocities, $k_{obs,fast}$ was used in the following. It is referred to as k_3' or k_4', where k_4' is the limiting value of the reduction rate of nucleotide-bound BCR_{ox} (see below). This is considered legitimitate as our following analysis relies solely on the ratios of k_3' and k_4'; in all cases, similar results were obtained with initial velocities instead of k_3' and k_4'.

The slow phase of BCR reduction by dithionite was independent of the dithionite concentration and was determined to be 0.35 ± 0.05 s^{-1} from several data sets; furthermore, it was not significantly changed in the presence of substrates. At present, we have no quantitative explanation for this kinetic heterogeneity. Little importance is attributed to the slow phase as the results described below rest solely on the fast phase of dithionite reduction.

Reduction Kinetics of Oxidized Benzoyl-CoA Reductase in the Presence of Saturating Amounts of Nucleotides and BCoA. In SFS experiments, oxidized BCR was incubated with saturating amounts of its substrates prior to reduction by dithionite (256 μM). The dithionite syringe contained an equal amount of substrate to prevent complex dissociation. Both MgATP and MgADP diminished the reduction rate significantly to 21% (k_{+4}[ATP] determined at 250 μM MgATP) and 25% (k_{+4}[ADP] determined at 2 mM MgADP) relative to the ligand-free enzyme. A typical set of reaction traces is shown in Figure 4A; the individual rate constants are summarized in Table 1. In contrast, the presence of 200 μM BCoA had only a slight effect (k_{+4}[BCoA], 93% of the ligand-free rate; Figure 4A). As BCoA showed no specific binding to the coenzyme A thiol ester site in the absence of MgATP or MgADP, it is likely that this small effect is due to some unspecific binding to the nucleotide binding site (see below).

To test whether the nucleotide-induced change in reduction rate might be due to an altered $E^{\circ\prime}$ of the clusters undergoing reduction, SFS experiments were performed in which BCR_{red} was mixed with substrates (both syringes contained equal amounts of dithionite; Figure 4A). Changes in the extent of absorption could be observed neither at 410 nm nor at 314 nm (dithionite), indicating that binding of ADP, ATP, and BCoA did not issue further cluster reduction. This finding is in accordance with the results from previous EPR experiments (*4*, *5*). The nucleotide-dependent changes associated with the altered reduction kinetics of BCR are referred to as a transition from BCR(nucleotide) to BCR*-(nucleotide) in the following.

Affinity and Stoichiometry of Nucleotide Binding Determined by SFS. To further characterize the nucleotide-dependent changes, the difference in the reduction rates of nucleotide-ligated vs ligand-free enzyme was used to measure the binding affinities of ADP and ATP to BCR_{ox}. In SFS experiments, BCR_{ox} was equilibrated with varying nucleotide concentrations prior to mixing with dithionite (100 μM after mixing). Both the BCR_{ox}- and the dithionite-containing syringes contained equal nucleotide concentrations in order to prevent ligand dissociation. The $k_{obs,fast}$ of reduction decreased with increasing ligand concentration and reached a constant value at concentrations higher than 50 μM ATP

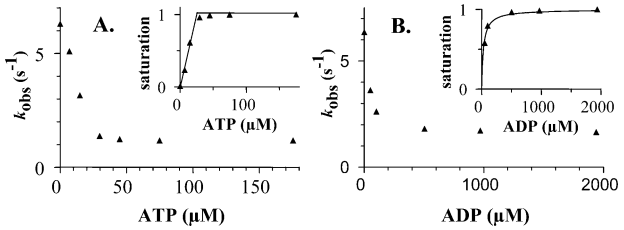

FIGURE 5: Effect of differing nucleotide concentrations on k_{obs} of BCR_{ox} reduction as determined by SFS. In SFS experiments, 20 μM BCR_{ox} was equilibrated with nucleotide prior to reduction by 100 μM dithionite. The same concentration of nucleotide was included in both syringes. The k_{obs} of the fast phase of reduction are plotted against the nucleotide concentration (large graph). The insets show the saturation (see text) of the nucleotide binding effect. Note that all error bars are smaller than the points used to represent the data.

and 500 μM ADP (Figure 5). To obtain the binding affinities, the rates were transformed into a saturation function Y with $Y = (k_{obs} - k_3')/(k_4' - k_3')$ (insets of Figure 5), where k_3' and k_4' represent the pseudo-first-order rates of the reduction of BCR and BCR*(nucleotide), respectively; k_4' was taken as the asymptotic value of k_{obs} at high nucleotide concentration. Assuming that only the switch and not the nucleotide binding per se alters the redox properties (see scheme in Figure 7), Y gives the proportion of enzyme undergoing reduction via the switched, nucleotide-bound form. Because of the high affinities observed in these experiments, Y is a direct measure of the ratio of nucleotide-bound enzyme, $[BCR(ATP)]/[BCR]_0$.

The binding constants (K_d) for MgATP and MgADP determined by SFS are referred to as $K_{d,1(SFS)}$(ATP/ADP) values in Table 1. Notably, they largely differed from the steady-state affinities determined in an earlier study where they were interpreted as apparent K_m(ATP) and K_i(ADP) values (*3*, *4*). The $K_{d,1}$ for MgADP was 32 ± 3 μM by fitting the saturation curve to the general binding equation (eq 1; see Experimental Procedures). A Hill plot transformation was used to analyze the SFS binding data for ATP, yielding a $K_{d,1(SFS)} = 11 \pm 2$ μM; likewise, a Stokell plot gave a similar $K_{d,1(SFS)}$ of 8 μM. The high affinity for ATP additionally allowed a determination of the stoichiometry of ATP binding in the stopped-flow experiments. At the intersection of the two asymptotes (inset of Figure 5A), all ATP is bound and its concentration corresponds to $n[BCR]_0$. Considering the concentration prior to mixing, the stoichiometry was 1.2 ATP/enzyme, indicating that binding of only one nucleotide is responsible for the effect on the reduction rates. This is remarkable since BCR contains two similar ATP-binding sites and since equilibrium dialysis experiments revealed that BCR binds two nucleotides (see below). It implies that the two binding sites have differing affinities, designated as $K_{d,1}$ (high affinity) and $K_{d,2}$ (low affinity) in the following. Notably, only $K_{d,1}$ could be determined in the SFS experiment.

Surprisingly, the Hill plot (Figure 6) had a significantly nonunity slope approaching unity at high ATP concentrations (Hill coefficient 3.3 ± 0.2, ADP 2.8 ± 0.3). Such a pattern is usually interpreted as cooperative behavior. Notably, only one binding site is involved in this effect, whereas cooperativity requires the interaction of several binding sites. Considering that the values for $K_{d,1}$ obtained from SFS

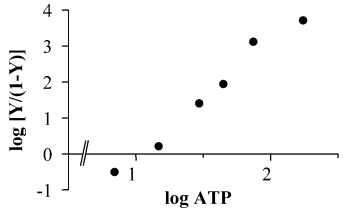

FIGURE 6: Hill plot analysis of ATP binding to BCR. A Hill plot of the saturation curve (Y) of ATP binding (Figure 5A) shows a pseudocooperative pattern with a significantly nonunity Hill coefficient of 3.3 ± 0.2. The $K_{d,1}$ is 11 ± 2 μM.

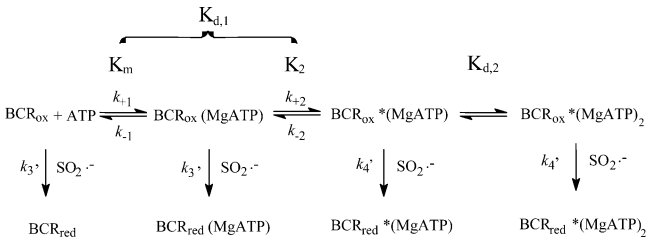

FIGURE 7: Scheme used for the interpretation of the reduction kinetics and nucleotide binding data of BCR. BCR* designates the conformation after the nucleotide-induced switch (for simplicity, we do not differentiate the conformations induced by different substrates). The constants k_1 and K_1 ($=K_m$) characterize the binding equilibrium, the constants k_2 and K_2 the switch, and k_3' and k_4' the reduction rates (the primes here indicate apparent values; for details see text).

differed by more than 1 order of magnitude from the steady-state values (see Table 1), we interpret this phenomenon as follows. The binding of a single nucleotide induces the conformational change described above from BCR to BCR*. The affinities of BCR ($K_1 = K_m$) and BCR* ($K_{d,1}$) for nucleotides differ largely with $K_1 \gg K_{d,1}$ (Figure 7). Accordingly, the pseudocooperative pattern in the Hill plot reflects the increase of the nucleotide binding affinity due to the increase of the overall affinity by the kinetically distinct switch step to $K_{d,1} = K_m/K_2$. For clarity, the following scheme is used for the interpretation of the data in this work. We distinguish between the following reactions: (i) binding of the first nucleotide to oxidized enzyme with K_1 corresponding to the observed K_m under steady-state conditions; (ii) a molecular switch from nucleotide-bound BCR_{ox} to nucleotide-bound BCR_{ox}* by k_2; (iii) reduction of BCR_{ox} and nucleotide-bound BCR_{ox} by k_3' or (iv) reduction of nucleotide-bound BCR_{ox}* by k_4'; and (v) binding of the second nucleotide to BCR_{ox}*(nucleotide) with $K_{d,2}$.

Kinetics of Nucleotide Binding and Nucleotide-Induced Switch. To estimate the kinetics of the nucleotide-induced switch (k_2), additional SFS experiments were performed. One syringe contained BCR_{ox}*(MgADP) which was mixed with a second syringe containing varying amounts of dithionite but no MgADP. Upon mixing, dilution forced the complex to dissociate with k_{-2}, thereby increasing the ratio of enzyme reduced with k_3' (nonswitched enzyme) versus k_4' (switched enzyme; Figure 7). As a result, the second-order rate increased from a mixture of k_3' and k_4' toward the pure k_3' as the limiting value (Figure 8A). [MgADP] was 200 μM; at this concentration maximal dissociation upon dilution was obtained (Figure 5B).

In the experiment described above, the switch from BCR_{ox}-(MgADP) to BCR_{ox}*(MgADP) is considered irreversible because of the fast dissociation equilibrium with BCR_{ox} and

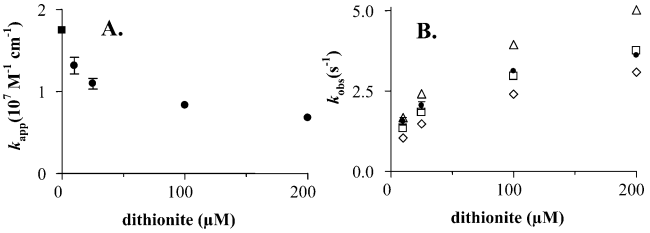

FIGURE 8: Kinetic competition between reduction and dissociation of the BCR_{ox}*(MgADP) as determined by SFS. One syringe contained a preequilibrated mixture of 20 μM BCR_{ox} and 200 μM MgADP; the other syringe contained varying concentrations of dithionite. (A) The second-order rate constants (●) approach k_3' (■) as the limiting value at very low dithionite concentrations. (B) The measured k_{obs} (●) was simulated using the kinetic scheme in Figure 7, the kinetic constants in Table 2, and $k_{-2} = 4\ s^{-1}$ (□). The k_{obs} simulated with $k_{-2} = 2\ s^{-1}$ (◇) and $k_{-2} = 10\ s^{-1}$ (△) give an estimate for the accuracy of simulation.

MgADP by k_{-1}. Typical rates for k_{-1} in MgADP dissociation are in the range of several 1000 s^{-1} (*28*, *29*), which justifies the assumption made above because the equilibrium of nucleotide binding is much faster than the nucleotide-induced switch. The k_{obs} could be simulated at a sufficient accuracy using $k_{-2} = 4\ s^{-1}$ (Figure 8B). Using different values for k_{-2}, the error can be estimated to be in the order of $\pm 1\ s^{-1}$. In a similar experiment with ATP k_{-2} was slightly lower than the value obtained with ADP (Table 1).

The finding of a slow switch back is of importance for the catalytic cycle proposed in this work (Figure 10). While the forward, ATP-binding switch is a relatively fast step ($k_2 > 100\ s^{-1}$), the very low rate for the reverse, ADP-dissociation switch ($k_{-2} = 4 \pm 1\ s^{-1}$) represents a rate-limiting step in the overall catalytic cycle which is $\sim 1\ s^{-1}$ under the conditions of the experiment.

Equilibrium Dialysis Studies with MgATP and MgADP. As SFS experiments were restricted to binding to BCR_{ox} and as only the binding of one nucleotide could be measured by this technique, equilibrium dialysis studies were carried out to determine the stoichiometry of binding and the affinity of the nucleotides to BCR. Note that ATP binding could only be analyzed with oxidized BCR as the reduced enzyme exhibits a low intrinsic ATPase activity (*4*). To minimize any unspecific binding of MgADP to the BCoA binding site, the K_d values for MgADP to reduced enzyme were determined in the presence of saturating BCoA concentrations (0.2 mM). In all experiments the concentration of Mg^{2+} was kept constant at 10 mM since variations of the Mg^{2+}/nucleotide ratio in a range from 1.2 to 10 did not affect BCR activity.

The binding data (Figure 9A,B) were fitted to eqs 1−3 (see Experimental Procedures). In all cases, the accuracy of the fit increased on changing from eq 1 over eq 2 to eq 3; e.g., for ADP binding to BCR_{ox} r^2 was 0.92, 0.95, and 0.96, respectively. Results are summarized in Table 2. Scatchard plots indicated that nucleotides bound in a biphasic mode as shown in the insets of Figure 9. As in the SFS experiments, all $K_{d,1}$ values were at least 1 order of magnitude lower than the K_m/K_i values. The $K_{d,1}$ values determined by equilibrium dialysis for binding to BCR_{ox}, referred to as $K_{d,1(ED)}$, were 10 ± 5 μM (MgATP) and 28 ± 8 μM (MgADP), with a good agreement to the values obtained from SFS (Table 1). BCR bound maximally 2.2 ± 0.4 MgATP and 2.7 ± 0.5 MgADP (Figure 9A,B; Table 2).

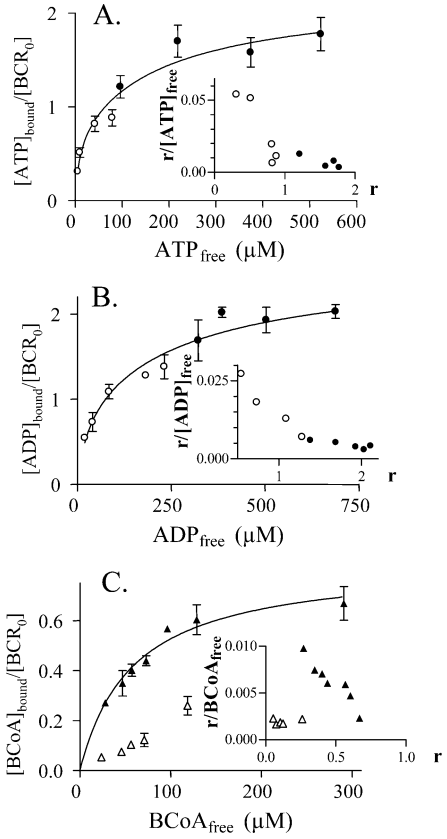

FIGURE 9: Equilibrium dialysis data of ATP, ADP, and BCoA binding to BCR. (A) ATP binding to BCR_{ox}. (B) ADP binding to BCR_{ox} (both in the presence of 0.2 mM BCoA and 2 mM DTE). (C) BCoA binding to BCR_{red} in the presence of 0.5 mM ADP (▲) and BCoA binding to BCR_{ox} (△); *r* is the proportion of ligand bound to total enzyme (=[BCR(ligand)]/$[BCR]_0$). The insets show the binding data in a Scatchard plot. The enzyme concentrations were 18 μM (○)/104 μM (●) in (A), 18 μM (○)/68 μM (●) in (B), and 51 μM (▲)/44 μM (△) in (C) (in the presence of 0.2 mM DTE).

Although slightly too high due to unspecific binding, the values are in accordance with predictions made from amino acid sequence analysis, which indicate the presence of two nucleotide binding sites per enzyme (*12*). The $K_{d,2(ED)}$ values could be determined by equilibrium dialysis and were 15−20-fold higher than the $K_{d,1(ED)}$ for BCR_{ox}; $K_{d,2(ED)}$MgADP was lower for BCR_{ox} than for BCR_{red} (Table 2). The results confirm that BCR has two binding sites of differing affinities which are occupied sequentially, as indicated by SFS experiments.

Equilibrium Dialysis Studies with Benzoyl-CoA. To determine the binding properties of BCoA, equilibrium dialysis experiments were performed by varying the redox state and coligand. The binding data were analyzed by fitting the data to eq 1 (Experimental Procedures). Surprisingly, binding of BCoA strictly depended on both the dithionite-reduced state of BCR and the presence of saturating amounts of nucleotide. Only under these conditions ~1 binding site with a K_d of 58 ± 10 μM was found (Figure 9C). The pattern of BCoA binding to BCR_{ox} was linear in the direct plot, and the corresponding Scatchard plot (inset of Figure 9C) had a zero slope, indicating an unspecific binding (e.g., to the nucleotide binding site). The accordance of the K_d value with the previously determined K_m of 37 μM (*6*) indicates that, in contrast to nucleotide binding, the binding mode of BCoA is similar under steady-state and nonturnover conditions. The

Table 2: Stoichiometry and Affinity of MgATP, MgADP, and Benzoyl-CoA Binding to Benzoyl-CoA Reductase As Determined from Equilibrium Dialysis Data

ligand	condition[a]	$K_{d,1}$ (μM)	$K_{d,2}$ (μM)	n_1	n_2
ATP	BCR_{ox}, no BCoA	10 ± 5	192 ± 45	0.8 ± 0.1	1.4 ± 0.3
ADP	BCR_{ox}, 0.2 mM BCoA	28 ± 8	313 ± 63	1.1 ± 0.2	1.5 ± 0.3
ADP	BCR_{red}, 0.2 mM BCoA	12 ± 7	528 ± 93	1.1 ± 0.2	1.8 ± 0.3
BCoA	BCR_{ox}, 5 mM ADP	$\gg 1000$		*b*	
BCoA	BCR_{ox}, no nucleotide	$\gg 1000$		*b*	
BCoA	BCR_{red}, 5 mM ADP	58 ± 10		0.9 ± 0.1	
BCoA	BCR_{red}, no nucleotide	$\gg 1000$		*b*	

[a] Experiments with BCR_{ox} included 2 mM DTE; with BCR_{red}, 1 mM dithionite. [b] Unspecific binding; e.g., $r \sim 0.2$ at [BCoA] = 100 μM.

factor of ~1.5 between the two values might be due to the fact that under steady-state conditions BCoA binds preferentially to BCR_{red}*(MgATP). The significant dependence of the affinity of BCoA to the reduced, nucleotide-bound state of BCR is yet another evidence for a nucleotide-induced switch.

DISCUSSION

In this work, a so far unknown nucleotide-dependent molecular switch has been detected in BCR catalysis as evidenced as follows: (i) the reduction rate of one or more [4Fe-4S] clusters was significantly diminished in the nucleotide-bound state of BCR, (ii) the binding of BCoA to the reduced enzyme strictly depended on bound nucleotide, and (iii) the pre-steady-state affinities of nucleotide binding were largely increased. These pre-steady-state effects are considered as results of a single molecular switch which depends on the binding of a nucleotide. With respect to BCoA binding, the result of this switch is a conversion of BCR from a closed to an open conformation. In contrast to the well-described high-spin/low-spin transition (from $S = {}^1/_2$ to $S = {}^7/_2$; *4*, *5*), the switch characterized in this work solely depends on binding but not on hydrolysis of ATP. Therefore, we distinguish between an "ATP-binding switch" and an "ATP-hydrolysis switch". Both switches contribute to the mechanism that converts chemical potential of ATP into redox potential. So far, the only enzymes known to catalyze ATP-driven electron transfer are BCR, 2-hydroxyglutaryl-CoA dehydratase, and nitrogenase (*7*, *30*−*32*). These enzymes share similarities in their overall design that make the distinction of a reductase and an activase module in BCR useful. However, BCR differs substantially from the former enzymes in respect to how it utilizes the energy of ATP hydrolysis to drive electron transfer, reflecting the particular needs of the underlying reaction mechanism. The following discussion highlights the similarities of the ATP-binding switch to other enzymes of the ASKHA-ATP binding motif family, as well as the differences to the ATP-binding switch of nitrogenase (related to G-proteins containing a Walker A ATP-binding motif). This comparison is an example of how divergent evolution has arrived at using different means to solve similar mechanistic problems.

Analysis of the SFS and equilibrium dialysis experiments showed that the two nucleotide binding sites of BCR are occupied sequentially (Figure 7). This binding pattern is evidenced by the observation that (i) only the binding of one ATP induced the change in reduction properties (i.e., the switch from BCR to BCR*), and the binding of the second ATP showed no detectable effects; (ii) equilibrium dialysis data of nucleotide binding displayed a biphasic pattern that fitted best to a sequential binding model; the $K_{d,1}$ of this analysis was in good agreement with the value obtained from SFS experiments; and (iii) Hill plot analysis of SFS nucleotide binding data showed a pseudocooperative pattern suggesting the presence of an intervening step that alters the overall affinity.

The sequential binding model represented in Figure 7 is able to explain why the nucleotide binding affinities measured in steady-state and pre-steady-state conditions differed by more than 1 order of magnitude (Table 1). Under steady-state conditions, BCR and BCR* states are in equilibrium, and hence only the initial binding step is measured (corresponding to K_m/K_i). In pre-steady-state conditions, however, the enzyme is essentially in the nonswitched state prior to binding. The nucleotide binding switch draws the overall equilibrium to the nucleotide-bound, switched form by depleting the initial binding equilibrium. The two successive binding equilibria result in the high overall affinity (represented by $K_{d,1} = K_m/K_2$) as shown in SFS and equilibrium dialysis experiments.

Other members of the ASKHA family (carrying the same ATP-binding motif; *11*) are reported to have a highly similar ATP-binding switch: in all cases, ATP binding induces a conformational change in two kinetically distinct binding and switch steps. The switch increases the overall affinity of nucleotide binding and is kinetically resolved from succeeding ATP-hydrolysis events (*33*−*35*). However, BCR differs from other members of the ASKHA family in that it contains two instead of only one ATP-binding site. The asymmetric, sequential nucleotide binding pattern of BCR can be rationalized by the asymmetry of the heterodimeric activase module (subunit A, 49 kDa, and subunit D, 29 kDa; Figure 2) and subtle differences of the two ATP-binding motifs (*12*).

In contrast, the ATP-binding sites of Fe protein (*30*, *31*) and activase from *Acidaminococcus fermentans* (*7*, *10*, *32*), respectively, are identical; both proteins are homodimers. Accordingly, the simultaneous binding of two ATP to the Fe protein of nitrogenase shows a cooperative pattern (*29*), and with dithionite as reductant both ATP are hydrolyzed for each electron transferred.

Noticeable differences between BCR and nitrogenase exist also in the effect of the nucleotide binding switch on the redox properties. Our results showed that in BCR not a single cluster but two interacting clusters become reduced by dithionite. These are most likely the electron entry cluster ligated by the A- and D- subunit and another cluster of the reductase module (clusters I and II; Figure 2). While ATP binding decreases the rate of reduction in both cases, the effect is rather modest in BCR as compared to Fe protein, where reduction of the nucleotide-bound state is slowed by

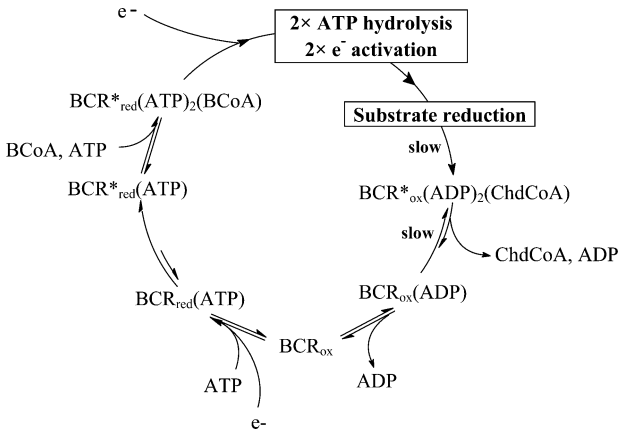

FIGURE 10: Proposed catalytic cycle of benzoyl-CoA reductase. BCR* denotes the switched state of the enzyme. Note that for complete BCoA reduction BCR has to be reduced by two electrons which both are ATP-dependently transferred to the aromatic ring. For details see Discussion.

3 orders of magnitude (*29*). This is in accordance with the absence of an effect of nucleotide binding on the redox potential of the interacting clusters in BCR. In contrast, nucleotide binding reduces the redox potential of the [4Fe-4S] cluster of Fe protein by 120 mV (MgATP) and 170 mV (MgADP) (*29*, *36*). Note that the major electron-activating event in BCR is the low-spin/high-spin switch of a $[4Fe\text{-}4S]^{+}$ cluster rather than gating of electrons between subunits.

The data obtained in this study allow completion of some missing links in earlier proposals of the catalytic cycle of BCR (*13*, *14*). Note that hydrolysis of two ATP and two electron transfers are necessary to complete each cycle. Therefore, after completing one cycle of substrate reduction, the enzyme will be in its switched, oxidized, and product-bound state [$BCR^{*}_{ox}(ADP)_2$(ChdCoA); Figure 10]. The slow reverse switch from BCR_{ox}* to BCR_{ox} will favor the accumulation of this resting state. This suggestion is supported by the observation that BCR is in the oxidized state in the steady state of catalysis under saturating concentrations of all substrates, despite an excess of dithionite (*4*). The product cyclohexa-1,5-diene-1-carbonyl-CoA (ChdCoA) will be readily released from the enzyme as oxidized BCR has only a poor affinity to thiol esters (see Table 2). To bind new ATP, BCR first needs to dissociate all bound ADP and accordingly revert to the nucleotide-depleted, nonswitched conformation. Kinetic simulations yielded an estimate for the reverse nucleotide dissociation switch of $k_{-2} = 4.0\ s^{-1}$, which places this step among the rate-determining steps, comprising approximately one-fourth of the catalytic cycle ($\sim 1\ s^{-1}$). In the unswitched state of BCR, a rapid equilibrium via the nucleotide-free enzyme achieves the nucleotide exchange followed by the rapid switch from BCR(MgATP) to BCR*(MgATP). Electron transfer to the enzyme and the binding of a second MgATP and BCoA restore the catalytically active complex BCR_{red}*(ATP_2)(BCoA). The next key events in the catalytic cycle of BCR were characterized previously: (i) ATP hydrolysis yielding an energy-rich enzyme−phosphate and ADP (*10*); (ii) the thermodynamically unfavorable low-spin/high-spin switch of a [4Fe-4S] cluster, most likely coupled to concomitant hydrolysis of the transiently formed enzyme−phosphate (*4*); (iii) two successive internal electron transfers to the substrate reduction site and complete BCoA reduction.

The ATP-binding switch characterized in this work stresses the role of ATP-induced conformational changes in the catalytic cycle of BCR. Apart from its role in electron activation, the binding of ATP affects the binding of the cosubstrate BCoA, the rate of enzyme reduction, and possibly the rate of internal electron transfer. The most remarkable aspect of the ATP-binding switch is the asymmetric design of the two ATP-binding sites, which provides the prerequisite for the activation of two electrons in one catalytic cycle.

ACKNOWLEDGMENT

We are grateful to Dr. Friedel Drepper for kindly providing two software packages and for helpful discussions.

REFERENCES

1. Boll, M., Laempe, D., Eisenreich, W., Bacher, A., Mittelberger, T., Heinze, J., and Fuchs, G. (2000) Non-aromatic products formed from anoxic conversion of benzoyl-CoA with benzoyl-CoA reductase and cyclohexa-1,5-diene-1-carbonyl-CoA hydratase, *J. Biol. Chem. 275*, 21889−21895.
2. Heider, H., Fuchs, G., and Boll, M. (2002) Anaerobic metabolism of aromatic compounds, *Curr. Opin. Biol. Chem. 6*, *604−611.*
3. Boll, M., and Fuchs, G. (1995) Benzoyl-coenzyme A reductase (dearomatizing), a key enzyme of anaerobic aromatic metabolism. ATP dependence of the reaction, purification and some properties of the enzyme from *Thauera aromatica* strain K172, *Eur. J. Biochem. 234*, 921−933.
4. Boll, M., Albracht, S. J. P., and Fuchs, G. (1997) Benzoyl-CoA reductase (dearomatizing), a key enzyme of anaerobic aromatic metabolism. A study of adenosinephosphate activity, ATP stoichiometry of the reaction and EPR properties of the enzyme, *Eur. J. Biochem. 244*, 840−851.
5. Boll, M., Fuchs, G., Meier, C., Trautwein, A., and Lowe, D. J. (2000) EPR and Mössbauer studies of benzoyl-CoA reductase, *J. Biol. Chem. 275*, 31857−31868.
6. Möbitz, H., and Boll, M. (2002) A Birch-like mechanism in enzymatic benzoyl-CoA reduction−a kinetic study of substrate analogues combined with an *ab initio* model, *Biochemistry 41*, 1752−1758.
7. Hans, M., Sievers, J., Müller, U., Bill, E., Vorholt, J. A., Linder, D., and Buckel, W. (1999) 2-Hydroxyglutaryl-CoA dehydratase from *Clostridium symbiosum*, *Eur. J. Biochem. 265*, 404−414.
8. Buckel, W., and Keese, R. (1995) One electron reactions of CoASH esters in anaerobic bacteria, *Angew. Chem., Int. Ed. Engl. 34*, 2398−2401.
9. Buckel, W. (1996) Unusual dehydrations in anaerobic bacteria: considering ketyls (radical anions) as reactive intermediates in enzymatic reactions, *FEBS Lett. 389*, 20−24.
10. Locher, K. P., Hans, M., Yeh, A. P., Schmid, B., Buckel, W., and Rees, D. C. (2001) Crystal structure of the *Acidaminococcus fermentans* 2-hydroxyglutaryl-CoA dehydratase component A, *J. Mol. Biol. 307*, 297−308.
11. Buss, K. A., Cooper, D. R., Ingram-Smith, C., Ferry, J. G., Sanders, D. A., and Hasson, M. S. (2001) Urkinase: structure of acetate kinase, a member of the ASKHA superfamily of phosphotransferases, *J. Bacteriol. 183*, 680−686.
12. Breese, K., Boll, M., Alt-Mörbe, J., Schägger, H., and Fuchs, G. (1998) Genes coding for the benzoyl-CoA pathway of anaerobic aromatic metabolism in the bacterium *T. aromatica*, *Eur. J. Biochem. 256*, 148−154.
13. Unciuleac, M., and Boll, M. (2001) Mechanism of ATP-driven electron-transfer catalyzed by the benzene ring-reducing enzyme benzoyl-CoA reductase, *Proc. Natl. Acad. Sci. U.S.A. 98*, 13619−13624.
14. Boll, M., Fuchs, G., and Lowe, D. J. (2001) Single turnover EPR studies of benzoyl-CoA reductase, *Biochemistry 40*, 7612−7620.
15. Meier, C. (2000) Mössbauerspektroskopie an biomimetischen Modellkomplexen und nicht-Häm-Eisenproteinen, Ph.D. Thesis, University of Lübeck, Germany.
16. Brackmann, R., and Fuchs, G. (1993) Enzymes of anaerobic metabolism of phenolic compounds−4-Hydroxybenzoyl-CoA reductase (dehydroxylating) from a denitrifying *Pseudomonas* species, *Eur. J. Biochem. 213*, 563−571.

17. Schachter, D., and Taggert, J. V. (1953) Benzoyl coenzyme A and hippurate synthesis, *J. Biol. Chem. 203*, 925−933.
18. Ziegler, K., Buder, R., Winter, H., and Fuchs, G. (1987) Studies on the anaerobic degradation of benzoic acid and 2-aminobenzoic acid by a denitrifying *Pseudomonas* strain, *Arch. Microbiol. 149*, 62−69.
19. Ryle, M. J., Lanzilotta, W. N., Mortenson, L. E., Watt, G. D., and Seefeldt, L. C. (1995) Evidence for a central role of lysine 15 of *Azotobacter vinelandii* nitrogenase iron protein in nucleotide binding and protein conformational changes, *J. Biol. Chem. 270*, 13112−13117.
20. Dawson, R. M. C., Eliott, D. C., Eliott, W. H., and Kenneth, M. J. (1986) in *Data for Biochemical Research*, 3rd ed., Clarendon Press, Oxford.
21. Webster, L. T., Mieyal, J. J., and Siddiqui, U. A. (1974) Benzoyl and hydroxybenzoyl esters of coenzyme A. Ultraviolet characterization and reaction mechanisms, *J. Biol. Chem. 249*, 2641−2645.
22. Bradford, M. M. (1976) A rapid and sensitive method for the quantitation of microgram quantities of protein utilizing the principle of protein-dye binding, *Anal. Biochem. 72*, 248−254.
23. Laemmli, U. K. (1970) Cleavage of structural proteins during the assembly of the head of bacteriophage T4, *Nature 227*, 680−685.
24. Rasmussen, T., Scheide, D., Brors, B., Kintscher, L., Weiss, H., and Friedrich, T. (2001) Identification of two tetranuclear FeS clusters on the ferredoxin-type subunit of NADH:ubiquinone oxidoreductase (complex I), *Biochemistry 40*, 6124−6131.
25. Lambeth, D. O., and Palmer, G. (1973) The kinetics and mechanism of reduction of electron-transfer proteins and other compounds of biological interest by dithionite, *J. Biol. Chem. 248*, 6095−6103.
26. Thorneley, R. N. (1975) Nitrogenase of *Klebsiella pneumoniae*. A stopped-flow study of magnesium-adenosine triphosphate-induce electron transfer between the component proteins, *Biochem. J. 145*, 391−396.
27. Thorneley, R. N., Yates, M. G., and Lowe, D. J. (1976) Nitrogenase of *Azotobacter chroococcum*. Kinetics of the reduction of oxidized iron-protein by sodium dithionite, *Biochem. J. 155*, 137−144.
28. Hammes, G. G., and Hurst, J. K. (1969) Relaxation spectra of adenosine triphosphate-creatine phosphotransferase, *Biochemistry 8*, 1083−1094.
29. Ashby, G. A., and Thorneley, R. N. F. (1987) Nitrogenase of *Klebsiella pneumoniae*. Kinetic studies on the Fe protein involving reduction by sodium dithionite, the binding of MgADP and a conformation change that alters the reactivity of the 4Fe-4S centre, *Biochem. J. 246*, 455−465.
30. Howard, J. B., and Rees, D. C. (1996) Structural Basis of Biological Nitrogen Fixation, *Chem. Rev. 96*, 2965−2982.
31. Rees, D. C., and Howard, J. B. (2000) Nitrogenase: standing at the crossroads, *Curr. Opin. Chem. Biol. 4*, 559−566.
32. Hans, M., Bill, E., Cirpus, I., Pierik, A. J., Hetzel, M., Alber, D., and Buckel W. (2002) Adenosine triphosphate-induced electron transfer in 2-hydroxyglutaryl-CoA dehydratase from *Acidaminococcus fermentans*, *Biochemistry 41*, 5873−5882.
33. Theyssen, H., Schuster, H. P., Packschies, L., Bukau, B., and Reinstein, J. (1996) The second step of ATP binding to DnaK induces peptide release, *J. Mol. Biol. 263*, 657−670.
34. Silberg, J. J., and Vickery, L. E. (2000) Kinetic characterization of the ATPase cycle of the molecular chaperone Hsc66 from *Escherichia coli*, *J. Biol. Chem. 275*, 7779−7786.
35. Ha, J. H., and McKay, D. B. (1995) Kinetics of nucleotide-induced changes in the tryptophan fluorescence of the molecular chaperone Hsc70 and its subfragments suggest the ATP-induced conformational change follows initial ATP binding, *Biochemistry 34*, 11635−11644.
36. Watt, G. D., Wang, Z. C., and Knotts, R. R. (1986) Redox reactions of and nucleotide binding to the iron protein of *Azotobacter vinelandii*, *Biochemistry 25*, 8156−8162.

BI0358871